Journal of Wind Engineering & Industrial Aerodynamics 184 (2019) 305–312

Contents lists available at ScienceDirect

Journal of Wind Engineering & Industrial Aerodynamics

journal homepage: www.elsevier.com/locate/jweia

Experimental study of yaw angle effect on the aerodynamic characteristics of a road vehicle fitted with a rear spoiler

See-Yuan Cheng [a,b,*], Kwang-Yhee Chin [b], Shuhaimi Mansor [c], Abd Basid Abd Rahman [c]

[a] Centre for Advanced Research on Energy, Universiti Teknikal Malaysia Melaka, Hang Tuah Jaya, 76100, Durian Tunggal, Melaka, Malaysia
[b] Faculty of Mechanical Engineering, Universiti Teknikal Malaysia Melaka, Hang Tuah Jaya, 76100, Durian Tunggal, Melaka, Malaysia
[c] Faculty of Mechanical Engineering, Universiti Teknologi Malaysia, 81310, UTM Skudai, Johor, Malaysia

ARTICLE INFO

Keywords:
Spoiler
Yaw angle
Wake multistability
Bistability
Wake flow
Aerodynamics
Hatchback

ABSTRACT

This study investigates the yaw angle effect on the aerodynamic performance of a hatchback model fitted with a roof spoiler. Although the aerodynamic performance of road vehicles is highly dependent on its yaw angle, it has rarely been considered in studies pertaining to roof spoiler applications. Two common types of spoilers are studied, namely, strip and wing types. The hatchback model is based on the Ahmed body at 35° slant angle. The yaw angle affects the aerodynamic performance of the hatchback model negatively regardless of the presence of a spoiler. However, the impact is more pronounced with the absence of a spoiler, particularly at higher yaw angles. Most importantly, the use of a spoiler prevents the bi-stability behaviour of flow which occurred in the model without the spoiler. Furthermore, the strip spoiler reduces both the drag and lift coefficients (C_d and C_l), whereas the wing type results in a greater reduction in C_l while penalising C_d. The results of the surface pressures indicate that the changes in the flow around the rear slanted body are the main factors affecting the aerodynamic performance of the hatchback model using the spoiler.

1. Introduction

In automotive aerodynamics, flow controls are normally applied to reduce the amount of drag or/and lift. Since road vehicles are of a blunted body shape, the aerodynamic forces encountered are dominated by the pressure components while skin friction is of lesser concern. Therefore, flow control applications in automotive aerodynamics typically focused on suppressing or delaying separation, and the control of large coherent structures at the rear part of vehicles.

Various passive devices have been successfully applied to improve the aerodynamic properties of road vehicles either in their simplified forms or complex geometries. For example, the use of deflectors at the side and leading edges of the rear slanted surface of a simple hatchback body (Hanfeng et al., 2016; Fourrié et al., 2011) or at the top of the forebody of a basic truck shape (Chowdhury et al., 2017). Also, vortex generators at the rounded rear section (Aider et al., 2010) or near the end of the roof (Pujals et al., 2010) of simple bodies; cavity at the base of a simple squareback body (Bonnavion and Cadot, 2018; Lucas et al., 2017; Bonnavion et al., 2017a; Evrard et al., 2016); rounded edge for location where flow separation is anticipated (Thacker et al., 2012); as well as the use of rear wing and spoiler for a basic car shape (Tsai et al., 2009) and production car (Gerhardt et al., 1981). From among these, rear wings and spoilers are commonly found in real life applications.

Rear spoilers can be defined as aerodynamic devices that are usually added to the trailing edge of the roof or trunk deck of a vehicle to improve its aerodynamic performance. Primarily, the goal is to improve the downforce despite the subsequent drag penalty. Since downforce is proportional to tractive force, it is imperative for the ride's stability and safety. Furthermore, good downforce performance is vital during cornering when the vehicle needs sufficient traction for it to pass the curve without slipping.

Rear spoilers can generally be divided into simple strip and standing wing types. The effectiveness of rear spoilers in enhancing the aerodynamic performance of road vehicles has been of interest in numerous studies given factors such as fuel economy, ride stability, and reasons associated with race speed. Tsai et al. (2009) investigated the effect of the rear wing on the drag and lift coefficients (C_d and C_l) of a generic passenger car model. The Reynolds number of their study was 3.6×10^6, and they reported that the application of the rear wing reduced the C_l by ~200%, whereas, the C_d increased by ~20%. Furthermore, Daryakenari et al. (2013), reported a similar lift reduction tendency due to the rear wing effect. While Gerhardt et al. (1981) reported the application of the

* Corresponding author. Faculty of Mechanical Engineering, Universiti Teknikal Malaysia Melaka, Hang Tuah Jaya, 76100, Durian Tunggal, Melaka, Malaysia.
E-mail address: cheng@utem.edu.my (S.-Y. Cheng).

https://doi.org/10.1016/j.jweia.2018.11.033
Received 12 July 2018; Received in revised form 23 November 2018; Accepted 25 November 2018
Available online 8 December 2018
0167-6105/© 2018 Elsevier Ltd. All rights reserved.

spoiler, by combining the wing and strip configurations into one integrated design to optimise the aerodynamic performance of a Group-5 racing car. Moreover, they found that the strip configuration which acts similarly to the upper wing of a biplane prevented the separation of the flow downstream of the high suction peak of the rear wing. As a result, higher downforce is generated with lower lift-induced drag. Although strip-type spoilers lack the aerofoil profile, their inclination angle has a strong influence on their aerodynamics. In this context, Cheng and Mansor (2017a and 2017b) investigated the influence of changing the inclination angle of the strip-type spoiler of a hatchback vehicle and reported reductions in both the C_d and C_l of up to 10.7% and 488%, respectively, at an inclination angle of 0°. Furthermore, they confirmed that the spoiler at negative inclination angles (i.e. leading edge higher than the trailing edge) would produce undesirable effects. In particular, an increase in both the C_d and C_l.

Although the aerodynamic characteristic of road vehicles is a strong function of the yaw angle (e.g. Bello-Millán et al. (2016) and Meile et al. (2016)), most studies on rear spoilers and other passive devices did not include this factor. Of particular interest to this study is the bi-stability behaviour encountered by the Ahmed body with a 35° slant angle within a small yaw angle range (Bello-Millán et al. (2016) and Rao et al. (2018)). In this case, the bi-stable flow condition is characterised by switching of the near-wake flow of the body from an entirely separated flow over the entire rear slanted surface (referred to as flow state I) to a reattached flow topology (flow state II). The switching between these two flow topologies causes a dramatic change in the aerodynamic characteristics of the Ahmed body, particularly at the rear part.

The yaw angle effect is common in real driving conditions when vehicles encounter crosswinds or during cornering. However, it is unclear whether the recorded benefits of employing a spoiler remains valid in the circumstances involving yaw angle change, particularly for suppressing the bi-stability behaviour encountered by the uncontrolled configuration. Therefore, to address this question, the present study investigates the effect of varying the yaw angle on the aerodynamic performances of a vehicle model equipped with various rear spoiler configurations.

2. Methodology

2.1. Vehicle model

The present study has adopted the Ahmed body to investigate the aerodynamic characteristic of hatchback-type vehicles. The Ahmed body is a reference model introduced by Ahmed et al. (1984) to study the effect of the backlight angle on the aerodynamic drag characteristics and associated flows. In this study, the backlight angle was fixed at 35° as this is the typical angle found in most hatchback-type vehicles. For the wind tunnel test, the idealised hatchback model was fabricated as a 75% replica. Fig. 1 illustrates the dimensions of the scale-down Ahmed body and its body part designations at a 35° backlight angle configuration. The tolerance of manufacturing is ±2 mm, and it was built using wood with a surface roughness (Ra) of approximately 0.5–0.8 μm.

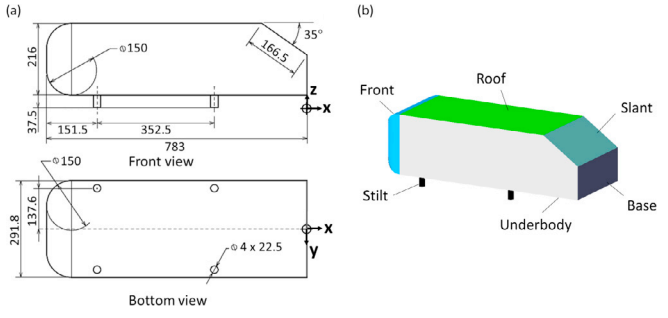

Fig. 1. (a) Ahmed body at 75% scale, and (b) the designations of body parts; dimensions are in millimeters.

2.2. Spoiler configurations

Two types of spoilers were investigated in this work, namely, the simple strip and standing wing (refer to Fig. 2; unit in millimeters). The latter used the NACA 0018 profile for simplicity of the geometric configuration, and the length c of the wing type was 51.75 mm while the maximum thickness was 9.32 mm. The size of its endplate was determined by first fixing the height where the rear wing should be mounted in proportion to the one typically found in real hatchbacks (e.g. Ford Focus RS and Proton Satria). Next, the endplate was created in such a way that its outer edges are slightly extended from the wing profile to prevent wingtip vortices from forming. The dimensions of the spoilers were obtained by scaling down the typical length of the rear-roof spoilers found in real vehicles. The inclination angle θ of all the spoilers was fixed at an angle of 5°. This angle was chosen based on the study of Cheng and Mansor, (2017b) indicating that the strip spoiler configured at this angle did not cause any significant increase in drag but generated sufficient downforce. Although relatively higher downforce was produced at higher spoiler angles, but the corresponding drag forces were also higher. For passenger cars, an increase in the drag value is not preferable due to the more and more stringent CO_2 emission legislations. The same angle was applied to the rear wing for consistency and comparative purposes.

The spoilers were built using wood, while the endplates of the rear wing were made of metal. During wind tunnel tests, the spoilers were mounted and attached to the hatchback model using metal screws.

2.3. Wind tunnel test configurations and measurements

The experiments were conducted in the low-speed wind tunnel at the Aeronautics Laboratory of University of Technology, Malaysia. The wind tunnel is a closed return type with a test section of 2.0 m (width) x 1.5 m (height) x 5.8 m (length). The maximum wind speed is ~80 m/s (i.e. Mach 0.23), and the non-uniformity of the flow is below 0.15% of the mean value. The mean degree of turbulence is lower than 0.06%.

The wind speed of all cases was fixed at 53 m/s, and the corresponding Reynolds number based on the length of the model was 2.7×10^6. This Reynolds number was chosen because a Reynolds number

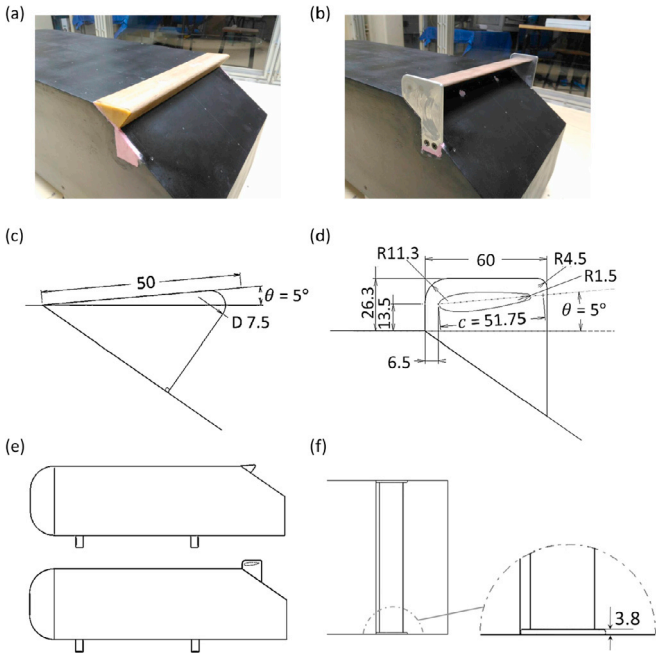

Fig. 2. Spoiler configurations; Photographs of strip (a) and wing (b), Dimensions of strip (c) and wing (d) in millimeters; (e) Side view of model mounted with the strip (above) and wing (below); (f) Top view of wing and the thickness of the endplate.

dependency test indicates that the aerodynamic forces had settled down at this Reynolds number value (Fig. 3). The drag coefficient values obtained by other experimental studies (i.e. Ahmed et al., 1984; Meile et al., 2011; Meile et al., 2016) were also plotted and shown in the figure for comparison. As shown in Fig. 3, they are in good agreement. The uniformity of the air velocity and temperature in the wind tunnel was digitally monitored.

The yaw angle is defined as the angle between the direction of airflow and the path of the vehicle. The yaw angle of the tests varied between 0 and 12°, in 2° increments. The maximum yaw angle was fixed at 12° because vehicles, at high speeds, rarely experience a higher yaw angle(s), (Cooper, 1985). For the model, the blockage ratio of the tests was 2.1% at a zero yaw angle, which increases to 3.2% at the yaw angle of 12°. Due to the rather small blockage ratios for the given yaw angle range, no correction factor was applied to the test results. Fig. 4 shows the convention of the yaw angle and the aerodynamic force coefficients. This paper adopted the body-axes-coordinate system, i.e. the C_d is parallel to the longitudinal axis of the model, while the C_l is perpendicular to C_d and pointing upward.

The model was mounted on the built-in turntable of the wind tunnel to allow the yaw angle to change and was lifted 140 mm from the wind tunnel floor to minimise the boundary layer effect. Then, a horizontal circular board, acting as the ground surface (also mounted on the turntable) was placed underneath the model for controlling the ground clearance distance (Fig. 4(a) and (b)). The distance from the leading edge of the circular board to the front of the model was 265 mm. Although the boundary layer thickness has not been measured, and since the surface of the board is smooth, it can be estimated by applying the one-seventh-power law. In this case, it should be approximately 6 mm thick by the time the flow reaches the front of the model. Given the underbody clearance is maintained at 37.5 mm (i.e. 31% of the base height), the influence of the boundary layer should be insignificant.

The model was connected to a six-component balance via four stilts to record the aerodynamic forces. The load cell is a 6 DoF force-torque sensor (model 160M50), manufactured by JR3 Inc., USA with an accuracy of 0.011% at full scale for all forces and moments, which corresponds to a margin of error of 0.3465 N for the measured forces. Moreover, it was mounted in order that it turns together with the model when the turntable is rotated. Therefore, the directions of the recorded forces and moments are readily available in the body-axes-coordinate system without the need for conversion. The software package LabVIEW, developed by National Instruments, USA was used for data recording and processing. After setting the wind speed to 53 m/s, it took about 1–2 min before the wind speed settle down and force-moment reading stabilized. Thus, we waited for around 3–5 min before recording the data. The data sampling for each test configuration was performed for a duration of 20 s at the rate of about 25–45 Hz, which resulted in about 500–900 data points. The reported force coefficients are the time-averaged value over this 20 s period. The variations in the period to period time-averaged C_d and C_l over a period of 10 s show less

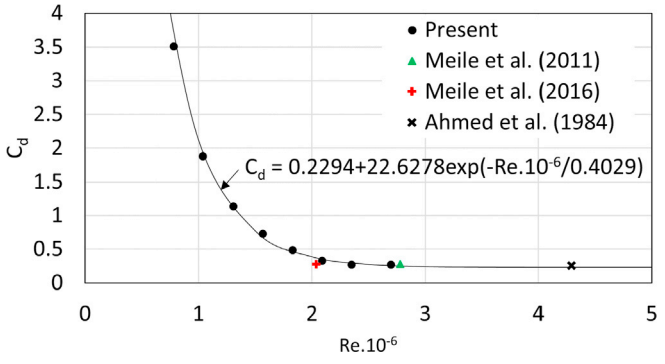

Fig. 3. Drag coefficient versus Reynolds number; Yaw angle = 0°.

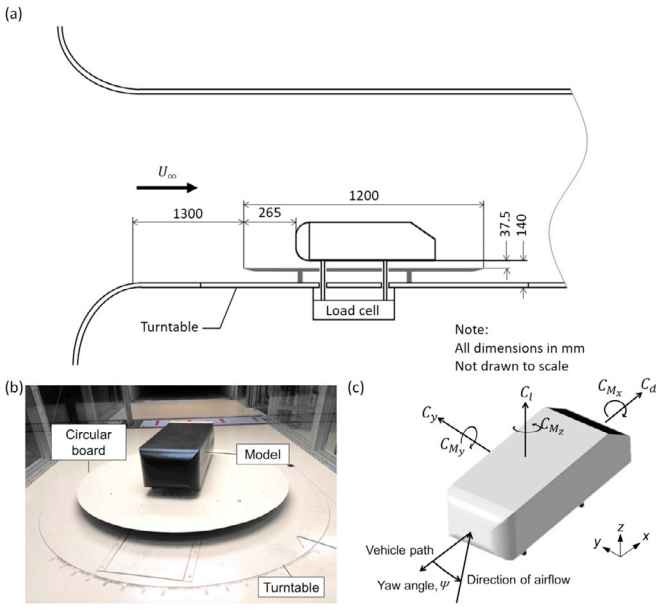

Fig. 4. Experimental set-up; (a) Schematic view of model in the test section; (b) Photograph of model in the test section; (c) Conventions of yaw angle and aerodynamic force and moment coefficients.

than 1% and 5% change, respectively, indicating that the mean values have converged.

The model was instrumented with pressure taps to record the surface pressure distribution at the rear section of the model. Fig. 5 shows the locations of the pressure taps. The majority of these locations were chosen in reference to Meile et al. (2016). However, some additional tapings were added around the end of the model's roof to allow examination of the influence of the rear spoilers on the surface pressure distribution around this region. Fig. 5 provides the exact coordinates of the pressure taps. In this case, the metering points (MP) 1–9 are located in the plane of y = 180 mm, MP 15–21 in the plane of y = 90 mm, MP 22–33 in the plane of y = 0 mm, MP 36–42 in the plane of y = −90 mm, and MP 43–51 in the plane of y = −180 mm. Accordingly, only the x and z coordinates of the MP are shown in Fig. 5.

Notably, when the strip-type spoiler was mounted, the surface pressure data at MP 4, 16, 25, 37, and 46 were unavailable due to the tapings being covered by the spoiler.

The MKS Baratron differential pressure sensors, (model 120AD-00100RCUS), which has a range of 4500 Pa, were used to probe the static pressure. The ambient pressure of the test section was used as the reference pressure. Meanwhile, the range of the transducer was within

MP#	x [mm]	z [mm]
1, 22, 43	-375	338
2, 23, 44	-295	338
3, 15, 24, 36, 45	-215	338
4, 16, 25, 37, 46	-164.28	325.69
5, 17, 26, 38, 47	-92.19	275.22
6, 18, 27, 39, 48	-20.11	224.74
7, 19, 28, 40, 49	0	165
8, 20, 29, 41, 50	0	125
9, 21, 30, 42, 51	0	65
31	-21	50
32	-116.77	50
33	-215	50

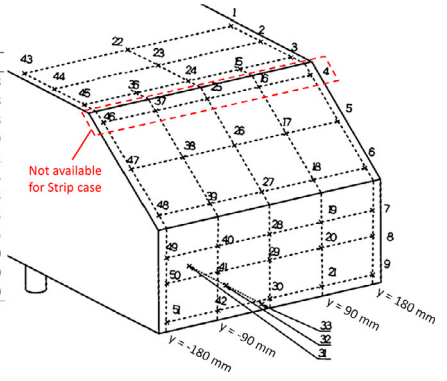

Fig. 5. Coordinates and locations of the pressure taps for surface pressure measurements. The origin of the coordinate system is located at the ground surface, aligned with the centreline of the base of the model.

±7 kPa. The pressure taps used have an outer diameter of 1 mm and an inner diameter of 0.5 mm. LabVIEW was used for data recording and processing.

3. Results and discussion

3.1. Effect of the yaw angle on C_d and C_l

Fig. 6 compares the influence of each spoiler type on the C_d, C_l, and pitching moment coefficient C_{my} of the hatchback model as a function of the yaw angle. In general, the yaw angle will have a negative impact on both the C_d and C_l regardless of whether the model comes with or without a spoiler. However, in baseline cases (i.e. without the spoiler); the influence of yaw angle on the two force coefficients becomes much worse beyond the yaw angle of 8° as evidenced by the surge of the two force coefficients. The sharp decline in C_{my} beyond the 8° yaw angle indicates that the surge of C_l is caused by the increase in rear axle lift. In Subsection 3.3, the C_p distribution results will show that the increase in rear axle lift is attributed to the drop in the surface pressure at the slant.

The discontinuous curve shape observed in the baseline case has also been reported by Meile et al. (2016), who investigated the influence of the yaw angle on the aerodynamic forces and moments of the Ahmed model with two different slant angles. In their study, they explained that the significant increase in the aerodynamic forces is caused by the change in the flow topology at the rear part of the model. Even with real hatchback vehicles, the sudden increase in the force coefficients at a particular high yaw angle range will occur (Bonnavion et al., 2017b). In these two studies, the critical yaw angles which correspond to the sudden increase in the force coefficients occurred at an angle of 12.5° (Meile et al., 2016) and 8.6° (Bonnavion et al., 2017b), respectively.

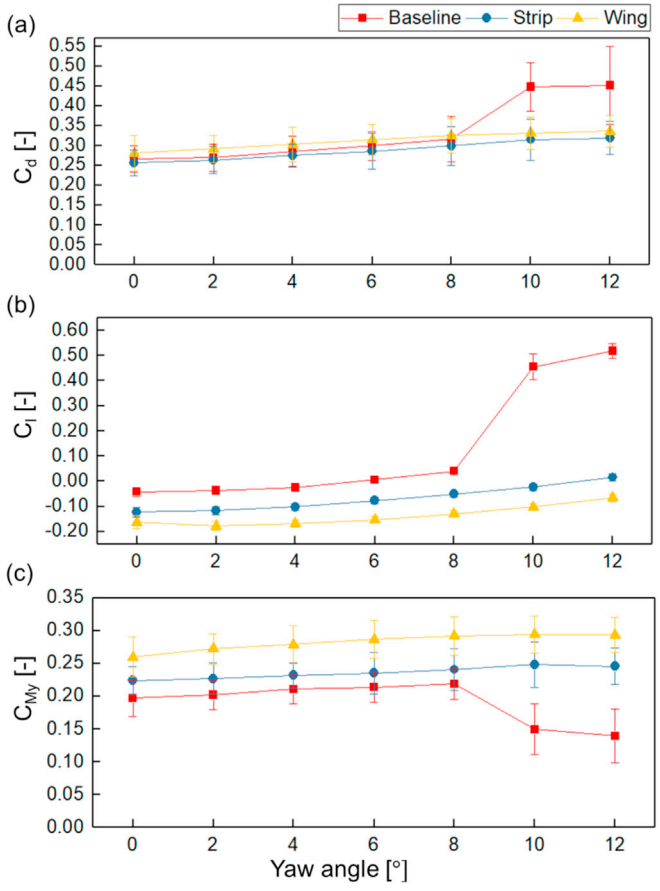

Fig. 6. Mean force and moment coefficients as a function of yaw angle; (a) C_d, (b) C_l, and (c) C_{my}; Error bars are standard deviation; Reynolds number = 2.7×10^6.

The baseline case is similar to the study of Meile at al. (2016), with a 35° back slant angle. However, in their study, they reported a larger critical angle. According to the mechanism proposed by Meile et al. (2016) and Bonnavion et al. (2017a,b), the significant increase in the force coefficients is caused by the reattachment of flow on the slant when the downwash-inducing, roof-edge vortices were sufficiently intensified by the yaw angle effect. Notably, a change in the aspect ratio of the model will also trigger similar reattachment of flow on the slant (Corallo et al., 2015). Rao et al. (2018) suggested several factors that could influence the wake occurring behind the Ahmed body, leading to the flow reattachment, which includes the Reynolds number and upstream disturbances. Although the Reynolds number used in the present study is slightly higher than the value used by Meile at al. (2016), the difference may not be significant enough to have caused the discrepancy. A more plausible factor is a symmetry defect which may be evidenced by the slight asymmetric surface C_p distributions on the left and right sides of the base and slant of the model at a zero yaw angle (Fig. 12(a), (e), and (i)). In this study, when the model was installed on the turntable, the model was manually aligned by referring to a reference line which is parallel to the freestream velocity for the zero yaw angle configuration. Any misalignment or geometrical imperfections of the model, in this case, would result in a symmetry defect in the flow. In some preliminary test cases, the C_d and C_l sweep for positive and negative yaw angles were obtained and found that the critical yaw angle values varied by about 4° between the negative and positive sides of the yaw angle (i.e. critical yaw angles occurred at −8° and 12°). Despite the C_d and C_l curves before the critical yaw angle being quite symmetric about the vertical axis at the yaw angle of 0°. Thus, the results indicate that the critical yaw angle is highly sensitive to any symmetry defects of the flow. Notwithstanding, the use of the scaled-down model in the present study could also have resulted in a configuration that is more sensitive to disturbances; thereby increasing the chance for the critical angle to occur earlier. Accordingly, further study would be needed to verify this hypothesis.

Nevertheless, the results obtained by the baseline case indicate that a change of the flow state exists at a particular yaw angle. Further, the absolute value of the critical yaw angle is highly sensitive to the flow condition and is subjected to a few degree variations from study to study despite the same Ahmed body with the same slant angle. For example, while the present experiment obtained the critical yaw angle within the range of 8°–12°, the results reported by Meile et al. (2016) show that the surge in the force coefficients occurred at the negative and positive yaw angles of −12° and 13°, respectively. Whereas, the numerical study by Rao et al. (2018) reported the occurrence of flow state II only when the yaw angle is increased to 15°.

The sudden increase in the two force coefficients at the high yaw angle did not occur in the with-spoiler cases. Thus, the results suggest that the surge of the force coefficients is ascribed to the change in the flow field at the rear section of the model, particularly the slant. This is confirmed by the C_p distribution as a function of the yaw angle, which is discussed in Section 3.3.

When comparing the standard deviations of C_d and C_l of all cases,

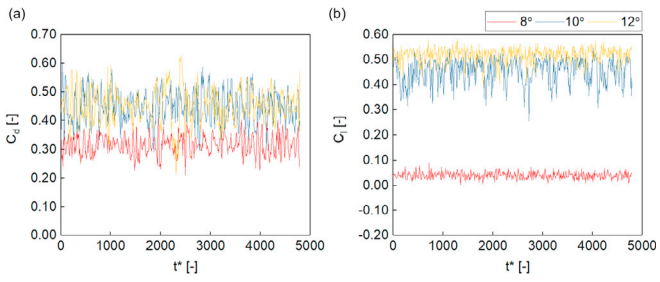

Fig. 7. Time series of C_d (a) and C_l (b) at different yaw angles; Baseline; Reynolds number = 2.7×10^6.

beyond the yaw angle of 8°, the model without the spoiler showed relatively large standard deviations. Fig. 7 shows the time-history of C_d and C_l at the critical yaw angle, and at the angles alongside it. For C_d, the time-series of 10° and 12° yaw seem to be very near to each other and show relatively large fluctuations as compared to the time-series of 8° yaw. Furthermore, their lower limit is right above the time-series of 8° yaw. As for C_l, the signal obtained at the critical angle shows the largest fluctuation with its upper limit located right below the time-series of 12° yaw. Moreover, its lower limit is quite far from the time-series of 8° yaw. If a smaller yaw angle increment was used, there is a possibility of capturing a time-series of the yaw angle right below the lower limit of the critical angle time-series. Nevertheless, the large fluctuations in C_d and C_l indicated that the model is subjected to more severe flow unsteadiness, particularly at the critical yaw angle.

However, when the rear spoiler is used (either strip or wing), apart from preventing the surge of the two force coefficients, the error bars which represent the level of fluctuation, were also smaller as compared to the corresponding values of the baseline case, thus indicating that the flow is steadier.

For yaw angles ranging between 0° and 8°, the strip spoiler showed an average reduction in C_d over the yaw angle by ~3.9%, while the wing caused the C_d to increase by an average of ~5.4%. However, in the high yaw angle regime (above 8°), the average reduction in C_d over the yaw angle in the strip and wing were ~29.6% and 25.8%, respectively.

As for C_l, both the strip and wing spoilers successfully reduced the value by ~168.7% and 319.6%, respectively. Although while all cases exhibited negative C_l at low yaw angles, the C_l value in the baseline case changed from negative to positive from yaw angles above 6°. However, this change was delayed to 12° when the strip spoiler was used. Finally, the model with a rear wing reported negative C_l throughout the yaw angle range tested. Indeed, it is well acknowledged that negative/lower lift will contribute to superior braking performance, high-speed stability, and cornering forces. Hence, the use of a rear wing is important, particularly for racing cars where performance is crucial.

3.2. Area-averaged C_p for the rear section of the model: effect of the spoiler

Fig. 8(a) compares the area-averaged C_p of the base, roof and slant between the baseline, strip and wing cases, at a zero yaw angle. As shown in the figure, the area-averaged C_p trend for the roof is well correlated to the C_l trend at the zero yaw angle. In particular, the wing case, which had exhibited the highest area-average C_p, showed the lowest C_l. This is expected as the higher surface pressure on the roof would mean less suction on the upper part of the model, resulting in a lower C_l.

As for C_d, a very good correlation was achieved with the area-averaged C_p trend of the slant. The strip case reported the highest area-averaged C_p, followed by the baseline case, and finally the wing case. Thus, the strip case reported the lowest C_d at a zero yaw angle, while the wing case reported the highest C_d. Again, such a tendency is expected given the higher surface pressure on the slant resulting in less suction on the back of the model. Hence, a model with a higher surface C_p on its slant has better potential to realise lower C_d.

Furthermore, no apparent correlation was found between the area-average C_p for the base and force coefficients. Although this fact may seem strange, but unlike the roof and slant, the differences in the area-averaged C_p between the three cases are relatively small for the base, therefore the influence on C_d and C_l is dominated by the roof and slant, not the base. Hence, one can surmise that at zero yaw angle the main factor that affects the aerodynamic forces by the use of spoiler is the modification in the flow field around the roof end and slant, i.e. the parts of the model near to the location where the spoiler is mounted. The same factor also applies to the small yaw angle range that is below the critical yaw angle.

3.3. Effect of the yaw angle on mean surface pressure distribution

Fig. 9 shows the mean surface pressure distributions of the with- and without-spoiler cases measured by the metering points placed along the centreline of the model (i.e. MP = 22–30) as a function of the yaw angle. For yaw angles below 10°, the shape of the C_p curves for the with- and without-spoiler cases are quite comparable to each other except for the roof end region where the C_p increases as the metering points are located nearer to the spoiler (i.e. more evident in the wing case). In contrast, the baseline case has a rather flat curve. Generally, the C_p value drops and settles at a lower range at the slant (i.e. MP = 25–27) and base (i.e. MP = 28–30). However, in the baseline and wing cases, the values at the base slightly increased.

As the yaw angle increases, the respective surface C_p value for each metering point decreased slightly. However, at high yaw angles of 10° and 12°, the surface C_p along the roof end and slant in the baseline case reported a significant drop. This trend observed in the baseline case agrees well with Meile et al. (2016) despite some differences in the

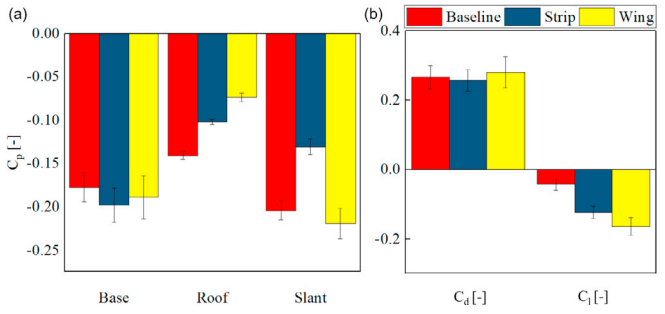

Fig. 8. (a) Impact of rear-roof spoiler on the area-averaged mean C_p of the roof, slant, and base; (b) Mean C_d and C_l; Yaw angle = 0°; Reynolds number = 2.7×10^6.

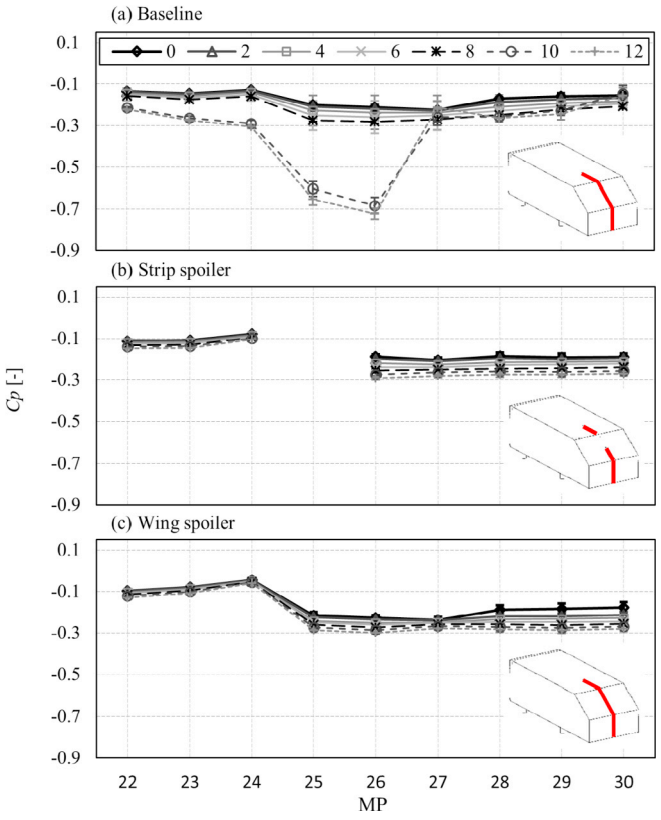

Fig. 9. Mean surface C_p distribution along the centerline of the roof end, slant, and base; Ψ = 0, 2, 4, 6, 8, 10, and 12°; Reynolds number = 2.7×10^6. (a) Baseline, (b) Strip, and (c) Wing.

obtained values (Fig. 10). In fact, the gaps are quite consistent particularly at yaw angles = 0° indicating that the discrepancy may be the result of differences in the experimental setting such as the Reynolds number, floor boundary layer treatment, etc. At yaw angles = 12°, the drop in the surface C_p around the slant is noticeably more pronounced in the present study which is attributed to the earlier occurrence of the critical yaw angle. The result of Meile et al. (2016) presented is slightly below the critical value.

The surface C_p contours for yaw angles equal to zero and around the critical value are depicted in Fig. 11 (base and slant) and 12 (roof and slant). In the baseline case, the relatively low surface C_p region near the windward edge of the slant could indicate an enhancement in the C-pillar vortex due to its merging with the roof-edge vortex. In addition, a significant decrease in the surface C_p of the entire slant is evident at the critical yaw angle. This tendency is the main reason for the sudden increase in the rear axle lift obtained from the baseline case discussed in Subsection 3.1. Previous studies have shown that the decrease in the slant surface pressure is caused by reattachment of the flow, separated from the top edge of the slant (e.g. Meile et al. (2016), Bonnavion et al. (2017b) and Rao et al. (2018)) when the flow switches from one state (fully separated flow over the slant) to another (reattachment of flow on the slant).

When a spoiler is used (either strip or wing), the change in the surface C_p of the rear part of the model is rather small for the yaw angle before and after the critical value. Moreover, the roof end surface C_p obtained from the with-spoiler cases is significantly larger than the baseline case and is free from the low surface pressure region near the trailing edge of the roof. Also, the upper part of the windward edge of the slant is absence of the low surface C_p region indicating that there is no (or weak) formation of a C-pillar vortex. Thus, the use of the spoiler prevented the reattachment of flow on the slanted face at the critical yaw angle observed in the baseline. Undoubtedly, this is the main reason why the force coefficients obtained from the with-spoiler cases are more stable over the yaw angle.

However, the real vehicle used in the study of Bonnavion et al. (2017b) exhibited a change in the flow state accompanied by a sudden increase in the force coefficients despite the use of a strip spoiler. In this case, a different spoiler angle could be the primary reason why the beneficial effect of the spoiler evidenced in the simple hatchback model was not reproduced in the real vehicle. Note that while the spoiler used in the present study was set at a 5° inclination angle, the spoiler used by the real vehicle is aligned with the roofline that slightly declines (i.e. with its trailing edge lower than the leading edge). Therefore, a marked difference found between their spoiler performances may be possible. Also, a real vehicle has more complicated forebody configurations. Accordingly, the A-pillar vortex generated in a real vehicle could further enhance the intensity of the C-pillar vortex when the two vortices interact with each other at the rear part of the vehicle (Cheng et al., 2013). Thus, increase the chances for the flow to reattach on the backlight of the vehicle at a critical yaw angle.

Fig. 13 shows the surface C_p obtained from the metering points located along the centreline near the end of the underbody. At low yaw angles, the curves of the surface C_p for all cases are decreasing, indicating that the surface pressure at the underbody is getting lower when approaching the rear end of the model.

Whereas, at high yaw angles, the surface C_p curves of the baseline cases are increasing. Thus, although the spoilers are mounted on the upper body of the model, their influence has somehow extended to the underbody flow. The use of a spoiler can affect the underbody flow because as it modifies the flow around the roof end, the wake will subsequently be modified. And since the wake is the downstream of the underbody flow, a change in the wake will also affect the underbody flow. In fact, the base surface C_p for the baseline case has become relatively high at the critical yaw angle (Fig. 11(c)). In addition, Meile et al. (2016) reported a lower flow velocity coming from the underbody clearance when the model is in a flow state of high force coefficients (i.e.

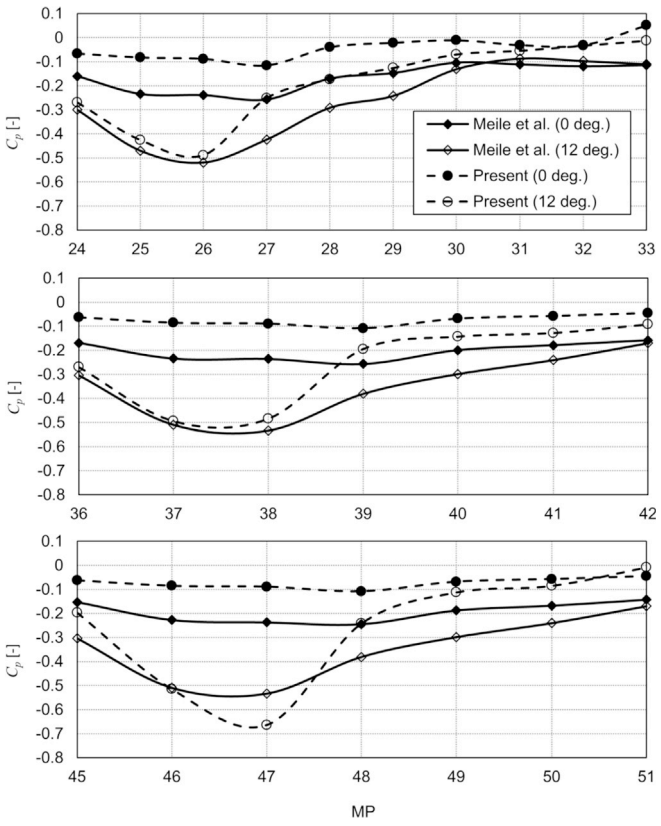

Fig. 10. Mean surface C_p distribution along the centerline of the roof end, slant, base, and underbody, as well as on one half of the roof end, slant, and base of Ahmed model; $\Psi = 0$ and 12°; Reynolds number = 2.7×10^6 (Present), and 2.0×10^6 (Meile et al., 2016).

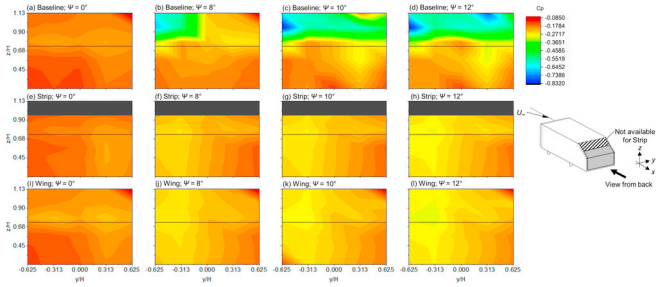

Fig. 11. Mean surface C_p distribution of the base and slant for yaw angles around the critical value; Baseline (a) $\Psi = 0°$, (b) $\Psi = 8°$, (c) $\Psi = 10°$, and (d) $\Psi = 12°$; Strip (e) $\Psi = 0°$, (f) $\Psi = 8°$, (g) $\Psi = 10°$, and (h) $\Psi = 12°$; Wing (i) $\Psi = 0°$, (j) $\Psi = 8°$, (k) $\Psi = 10°$, and (l) $\Psi = 12°$; State II occurred in (c) and (d); Reynolds number = 2.7×10^6; the lateral component of the freestream velocity is from left to right.

state II) (Figure 15 of Meile et al. (2016); y = 200–240 mm), indicating that the increase in the surface C_p of the underbody is influenced by the near wake flow.

Nevertheless, the increase in the underbody surface pressure of the baseline cases at high yaw angles is considered undesirable due to the potential rise in the pressure lift of the rear axle. As highlighted by Howell and Le Good (1999), higher rear axle lift is associated with vehicles with lower driving stability.

4. Conclusion

This study investigated the aerodynamic performances of a simplified hatchback model equipped with a rear-roof spoiler under the influence of

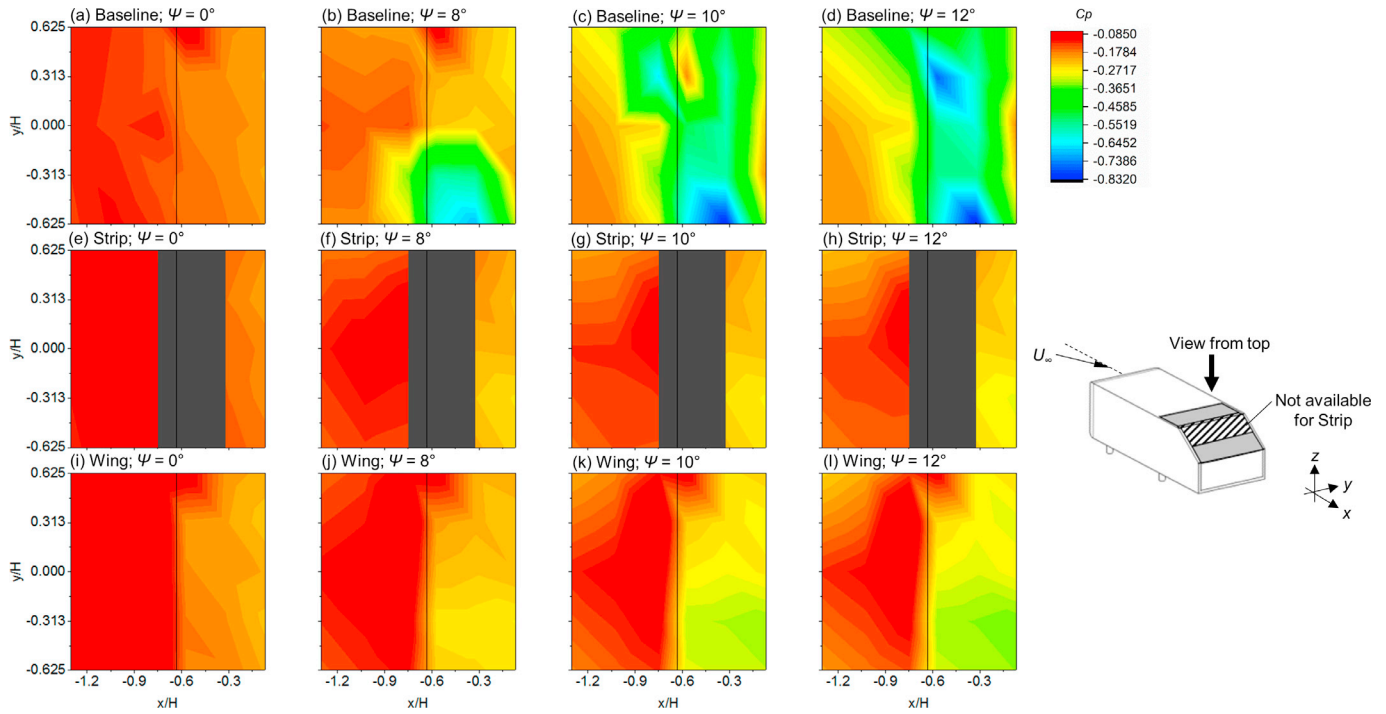

Fig. 12. Mean surface C_p distribution of the roof end and slant for yaw angles around the critical value; Baseline (a) $\Psi = 0°$, (b) $\Psi = 8°$, (c) $\Psi = 10°$, and (d) $\Psi = 12°$; Strip (e) $\Psi = 0°$, (f) $\Psi = 8°$, (g) $\Psi = 10°$, and (h) $\Psi = 12°$; Wing (i) $\Psi = 0°$, (j) $\Psi = 8°$, (k) $\Psi = 10°$, and (l) $\Psi = 12°$; State II occurred in (c) and (d); Reynolds number $= 2.7 \times 10^6$; the lateral component of the freestream velocity is from bottom to top.

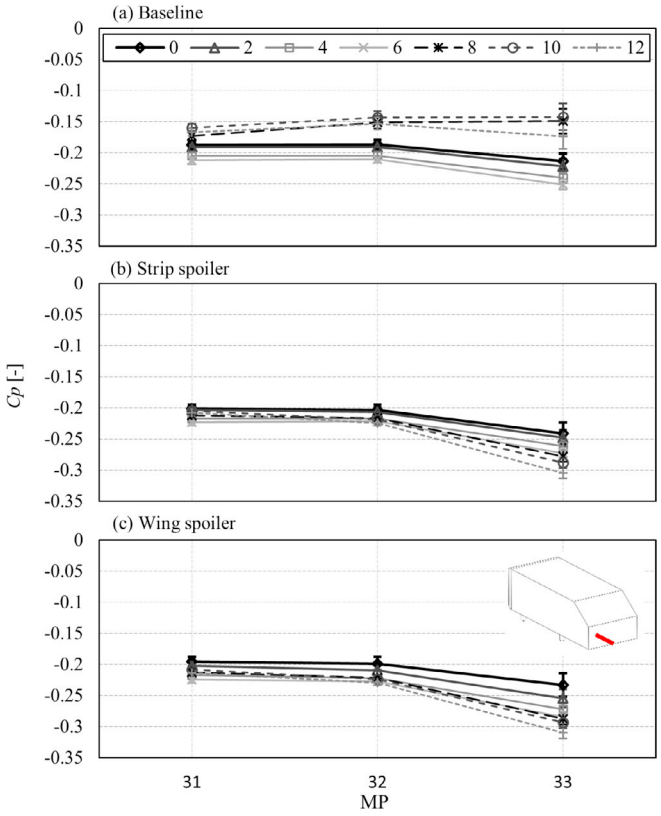

Fig. 13. Mean surface C_p distribution along the centerline of the end section of the model underbody; $\Psi = 0$, 2, 4, 6, 8, 10, and 12°; Reynolds number $= 2.7 \times 10^6$. (a) Baseline, (b) Strip, and (c) Wing.

yaw angles. Two spoiler types were tested; simple-strip and standing-wing. A model without a spoiler has also been tested, and the data served as the baseline. Wind tunnel experiments were also used to measure the aerodynamic forces and surface pressures and the length-based Reynolds number of the experiments was fixed at 2.7×10^6.

The yaw angle was found to have a negative influence on the aerodynamic performance of the hatchback model either with or without a rear roof spoiler. Apart from causing the C_d and C_l to increase, there is a critical value where the hatchback model would experience a dramatic increase in its aerodynamic forces associated with the change in the flow topology above its slanted rear surface. However, for the yaw angle range investigated, when either of the spoilers was employed, the worsening of such influence at the critical yaw angle (i.e. above 8°) abated. Simultaneously, the associated high level of flow unsteadiness also decreased due to the prevention of flow from switching between two distinct flow states (i.e. one producing high aerodynamic forces while the other producing low aerodynamic forces) within a particular yaw angle range.

From symmetric flow up to the moderate yaw angle conditions (i.e. 0–8°), the effect of the strip and wing on C_d is rather small. However, their influence on C_l is remarkable, especially on the wing. In particular, the reduction in C_l due to the strip and wing are respectively ~168.7% and 319.6%. Hence, vehicles demanding high performance would benefit from employing the rear wing.

Finally, despite a spoiler being mounted on the upper body of the model, its effect is traceable in the underbody flow due to modification of the wake flow, which could impact the driving stability characteristic.

Acknowledgement

The authors would like to thank Universiti Teknikal Malaysia Melaka (UTeM) and Ministry of Higher Education for supporting this research under FRGS FRGS/1/2015/TK03/FKM/02/F00273.

References

Ahmed, S., Ramm, G., Faltin, G., 1984. Some salient features of the time-averaged ground vehicle wake, in: SAE. p. 840300; 1-31.

Aider, J.L., Beaudoin, J.F., Wesfreid, J.E., 2010. Drag and lift reduction of a 3D bluff-body using active vortex generators. Exp. Fluid 48, 771–789. https://doi.org/10.1007/s00348-009-0770-y

Bello-Millán, F.J., Mäkelä, T., Parras, L., del Pino, C., Ferrera, C., 2016. Experimental study on Ahmed's body drag coefficient for different yaw angles. J. Wind Eng. Ind. Aerod. 157, 140–144. https://doi.org/10.1016/J.JWEIA.2016.08.005

Bonnavion, G., Cadot, O., 2018. Unstable wake dynamics of rectangular flat-backed bluff bodies with inclination and ground proximity. J. Fluid Mech. 854, 196–232. https://doi.org/10.1017/jfm.2018.630

Bonnavion, G., Cadot, O., Herbert, V., Parpais, S., Vigneron, R., Délery, J., 2017a. Effect of a Base Cavity on the Wake Modes of the Squareback Ahmed Body at Various Ground Clearances and Application to Drag Reduction.

Bonnavion, G., Cadot, O., Évrard, A., Herbert, V., Parpais, S., Vigneron, R., Délery, J., 2017b. On multistabilities of real car's wake. J. Wind Eng. Ind. Aerod. 164, 22–33. https://doi.org/10.1016/J.JWEIA.2017.02.004

Cheng, S.-Y., Mansor, S., 2017a. Influence of rear-roof spoiler on the aerodynamic performance of hatchback vehicle, in: Che Ghani, S.A., Wan Hamzah, W.A., Alias, A. (Eds.), MATEC Web of Conferences. EDP Sciences, p. 01027. https://doi.org/10.1051/matecconf/20179001027

Cheng, S.Y., Mansor, S., 2017b. Rear-roof spoiler effect on the aerodynamic drag performance of a simplified hatchback model. J. Phys. Conf. Ser. 822, 1–6. https://doi.org/10.1088/1742-6596/822/1/012008

Cheng, S.Y., Tsubokura, M., Okada, Y., Nouzawa, T., Nakashima, T., Doh, D.H., 2013. Aerodynamic stability of road vehicles in dynamic pitching motion. J. Wind Eng. Ind. Aerod. 122. https://doi.org/10.1016/j.jweia.2013.06.010

Chowdhury, H., Loganathan, B., Mustary, I., Moria, H., Alam, F., 2017. Effect of various deflectors on drag reduction for trucks. Energy Procedia 110, 561–566. https://doi.org/10.1016/j.egypro.2017.03.185

Cooper, K.R., 1985. The effect of front-edge rounding and rear-edge shaping on the aerodynamic drag of bluff vehicles in ground proximity. https://doi.org/10.4271/850288.

Corallo, M., Sheridan, J., Thompson, M.C., 2015. Effect of aspect ratio on the near-wake flow structure of an Ahmed body. Jnl. Wind Eng. Ind. Aerodyn. 147, 95–103. https://doi.org/10.1016/j.jweia.2015.09.006

Daryakenari, B., Abdullah, S., Zulkifli, R., Sundararajan, E., Sood, A.B.M., 2013. Numerical study of flow over ahmed body and a road vehicle and the change in aerodynamic characteristics caused by rear spoiler. Int. J. Fluid Mech. Res. 40, 354–372. https://doi.org/10.1615/InterJFluidMechRes.v40.i4.50

Evrard, A., Cadot, O., Herbert, V., Ricot, D., Vigneron, R., Délery, J., 2016. Fluid force and symmetry breaking modes of a 3D bluff body with a base cavity. J. Fluid Struct. 61, 99–114. https://doi.org/10.1016/j.jfluidstructs.2015.12.001

Fourrié, G., Keirsbulck, L., Labraga, L., Gilliéron, P., 2011. Bluff-body drag reduction using a deflector. Exp. Fluid 50, 385–395. https://doi.org/10.1007/s00348-010-0937-6

Gerhardt, H.J., Kramer, C., Ammerschläger, T., Fuhrmann, R., 1981. Aerodynamic optimization of a group-5 racing car. J. Wind Eng. Ind. Aerod. 9, 155–165. https://doi.org/10.1016/0167-6105(81)90086-6

Hanfeng, W., Yu, Z., Chao, Z., Xuhui, H., 2016. Aerodynamic drag reduction of an Ahmed body based on deflectors. J. Wind Eng. Ind. Aerod. 148, 34–44. https://doi.org/10.1016/j.jweia.2015.11.004

Howell, J., Le Good, G., 1999. The influence of aerodynamic lift on high speed stability. https://doi.org/10.4271/1999-01-0651.

Lucas, J.-M., Cadot, O., Herbert, V., Parpais, S., Délery, J., 2017. A numerical investigation of the asymmetric wake mode of a squareback Ahmed body – effect of a base cavity. J. Fluid Mech. 831, 675–697. https://doi.org/10.1017/jfm.2017.654

Meile, W., Brenn, G., Reppenhagen, A., Lechner, B., Fuchs, A., 2011. Experiments and numerical simulations on the aerodynamics of the ahmed body. CFD Lett.. 3, 32–38. https://doi.org/10.1017/CBO9781107415324.004

Meile, W., Ladinek, T., Brenn, G., Reppenhagen, A., Fuchs, A., 2016. Non-symmetric bi-stable flow around the Ahmed body. Int. J. Heat Fluid Flow 57, 34–47. https://doi.org/10.1016/J.IJHEATFLUIDFLOW.2015.11.002

Pujals, G., Depardon, S., Cossu, C., 2010. Drag reduction of a 3D bluff body using coherent streamwise streaks. Exp. Fluid 49, 1085–1094. https://doi.org/10.1007/s00348-010-0857-5

Rao, A., Minelli, G., Basara, B., Krajnović, S., 2018. On the two flow states in the wake of a hatchback Ahmed body. J. Wind Eng. Ind. Aerod. 173, 262–278. https://doi.org/10.1016/j.jweia.2017.10.021

Thacker, A., Aubrun, S., Leroy, A., Devinant, P., 2012. Effects of suppressing the 3D separation on the rear slant on the flow structures around an Ahmed body. J. Wind Eng. Ind. Aerod.. 107–108, 237–243. https://doi.org/10.1016/J.JWEIA.2012.04.022

Tsai, C.-H., Fu, L.-M., Tai, C.-H., Huang, Y.-L., Leong, J.-C., 2009. Computational aero-acoustic analysis of a passenger car with a rear spoiler. Appl. Math. Model. 33, 3661–3673. https://doi.org/10.1016/J.APM.2008.12.004